Topographic Effects on Barotropic Vortex Motion: No Mean Flow

HUNG-CHI KUO

Department of Atmospheric Science, National Taiwan University, Taipei, Taiwan

R. T. WILLIAMS

Department of Meteorology, Naval Postgraduate School, Monterey, California

JEN-HER CHEN AND YI-LIANG CHEN

Central Weather Bureau, Taipei, Taiwan

(Manuscript received 19 July 1999, in final form 23 October 2000)

ABSTRACT

The impact of the island topographic β effect on hurricane-like vortex tracks is studied. Both f plane and spherical geometry without a mean flow are considered. The simulations used in this study indicate the existence of a track mode in which vortices are trapped by the topography and follow a clockwise island-circulating path. The trapping of a hurricane-like vortex can be interpreted in terms of the influence of the island topographic β effect on the vortex track. Experiments on the f plane indicate that the drift speed along the clockwise path is proportional to the square root of $\beta_e v_{\max}$. The applicability of the square root law on the f plane is dependent on the degree to which the local β_e effect is felt by the vortex. The experiments on the sphere also demonstrate that the speed along the clockwise path is larger for a vortex with a larger maximum wind $v_{\max}$. The occurrence of hurricane-like vortex trapping, however, is not sensitive to the value of $v_{\max}$. When there is no background flow, the vortex will drift to the northwest in the presence of the planetary vorticity gradient. The β drift speed acts to keep the vortex from being trapped. The insensitivity of the vortex trapping to $v_{\max}$ on the sphere appears to be due to the possible cancellation of stronger planetary β and topographic β effects. The experiments suggest that the topographic scale must be comparable to (if not larger than) the vortex radius of maximum wind for the trapping to occur. Nonlinear effects are important in that they hold the vortex together and keep it moving without strong dispersion in the island-circulating path. This vortex coherency can be explained with the β Rossby number dynamics. The global shallow-water model calculations used in this study indicate that the vortex trapping increases with peak height, topographic length scale, and latitude (larger topographic β effect). In general, the trapping and clockwise circulating path in the presence of a planetary vorticity gradient will occur if the scale of the topography is greater than the vortex radius of maximum wind and if the planetary β parameter is less than the topographic β parameter.

1. Introduction

The problem of tropical cyclone forecasting is sometimes divided into two parts: intensity prediction and track prediction. At present, we seem to have little skill in predicting tropical cyclone intensity changes. Theoretical work (e.g., Hack and Schubert 1986) indicates that intensity changes are related to the relative spatial distributions of cumulus convection and inertial stability within the tropical cyclone. Others emphasize the importance of the approach of an upper-tropospheric synoptic scale trough (e.g., Molinari et al. 1998), the vertical wind shear over the tropical cyclone (e.g., DeMaria 1996), and the oceanic temperature on the hurricane intensity change (e.g., Bender et al. 1993). Thus, accurate intensity prediction requires a realistic interaction of moist physics and dynamics in a numerical model. Moreover, accurate treatment of air–sea interaction in a coupled model may be required for intensity prediction. Improved observational and data assimilation capability over the ocean as well as improved parameterization of the atmospheric boundary layer will help the cause.

The problem of track prediction, which is of considerable operational importance, is governed by an apparently complex interaction between the large-scale circulation in which the vortex is embedded and the vortex circulation itself. The dominant concept in the theory and forecasting of tropical cyclone motion is

Corresponding author address: Dr. R. T. Williams, Dept. of Meteorology, Naval Postgraduate School, 589 Dyer Road, Room 254, Monterey, CA 93943.
E-mail: rtwillia@nps.navy.mil

''steering'' by the environmental flow. In other words, typhoon track prediction can be viewed as a problem of accurately advecting a sharp peak in the potential vorticity field by a large-scale environmental background flow. In addition to the background steering flow, asymmetric circulations may result from the interaction of the vortex with the background absolute vorticity gradient. When there is no background flow, the vortex will drift to the northwest due to the interaction of the vortex with the planetary vorticity gradient (Adem 1956; McWilliams and Flierl 1979; Chan and Williams 1987). This is the so-called β-gyre effect (Fiorino and Elsberry 1989), where an asymmetric circulation is induced that advects the vortex. Carnevale et al. (1991) studied the propagation of barotropic vortex in a rotating tank and with a numerical model. They found that cyclones would spiral toward the top of the hill in an anticyclonic sense. This clockwise hill-circulating mode is argued to be similar to the β-gyre dynamics, which can be deduced from the rule of ''local northwest'' propagation of cyclones relative to contours of topography. There are also baroclinic effects that will affect the tropical cyclone motion. The baroclinic models of Shapiro (1992) and Flatau et al. (1994) strongly indicate that the motion of the tropical cyclone is governed by the dynamics of the lower cyclonic circulation. Namely, the cyclone moves relative to the background potential vorticity gradient as though it were a barotropic vortex with a vertically averaged wind profile. The diabatic processes also increase the vertical coupling. Thus, the first-order propagation effect in baroclinic conditions may be similar to the barotropic forecast.

Brand and Blelloch (1974) and Ishijima and Estoque (1987) studied the orographic effects on a westbound typhoon crossing Taiwan. Wang (1980) and Shieh et al. (1998) carried out the most comprehensive study of the Taiwan topographic effect on typhoon movement. After examining the behavior of more than 200 typhoons that threatened Taiwan between 1897 and 1996, Shieh et al. (1998) showed fifteen typical tracks for typhoons that crossed Taiwan. Figure 1 shows 9 of the 15 typhoon tracks from Shieh et al. (1998). The tracks are determined mainly from the surface data available in Taiwan. Interesting cases of discontinuous tracks (e.g., Typhoon Iris 1955; Typhoon B108 1925; Typhoon Kate 1962), of secondary lows on the lee (e.g., Typhoon Iris 1955; Typhoon Gilda 1962), and of continuous tracks (e.g., Typhoon Joan 1959; Typhoon Shirley 1960) are present. The thick dashed line for Typhoon Sarah (1989) is the track for a strong secondary low that was caused by the chinook wind on the eastern side of central mountain range. It is obvious from these historical cases (and many more similar recent cases), that the topography of Taiwan can affect the track of a typhoon. It is also interesting to see tracks parallel to the topography contours in some cases. Typhoons Bess and Sarah have clockwise paths, and Typhoon Kate's path is counterclockwise. Some important questions regarding a secondary low were not answered from the observational work. This is because Wang and Shieh's works involved subjective interpretations in which a mesoscale low-pressure center was often inferred from wind analysis based on the geostrophic relationship. This relationship may not be valid due to the presence of topography and the small spatial scales. The structure changes, and the effect of the secondary low formation have recently been addressed by Chang et al. (1993) using empirical orthogonal functions. They found that the spatial scale of the secondary low is significantly smaller than the scale of the low pressure that can be produced by an interaction of the mean steering flow and the topography.

These terrain-induced structure changes, track discontinuities, and secondary low or vortex formations are also evident in previous numerical simulations. The baroclinic modeling studies of Chang (1982) suggest that secondary vortex centers are formed on the lee side, as the vortex is blocked upstream by the mountain range. Lin et al. (1999) argued that the sudden increase of vorticity over the lee slope was associated with the generation of potential vorticity through the mechanisms of upstream blocking and wave overturning. Bender et al. (1987) compared simulations of tropical cyclones near islands in the Caribbean Sea, Taiwan, and Luzon in the Philippines. The maximum height is about 4300 m in Taiwan and 1500 m for the Philippines. Only in the Taiwan simulation was a secondary low formed; however, the secondary low center was simulated to occur much closer to the mountain peak as compared to the observational study of Chang et al. (1993). The Bender et al. high-resolution simulations produced more realistic intensity changes during typhoon approach, landfall, and departure from Taiwan. They also found that a region of dry air, which is due to the descending flow over land, is entrained into the cyclone and is responsible for the filling of the system before landfall. Thus, their results suggest that a slow-moving typhoon may start weakening several hours prior to landfall. Yeh and Elsberry (1993a,b) studied the upstream deflections as well as the continuous and discontinuous tracks for west-moving tropical cyclones passing Taiwan. The effect of the impinging angle to the island was also investigated by Yeh and Elsberry (1993b). They found that in agreement with the observation (e.g., Wang 1980; Shieh et al. 1998) vortices tend to track continuously around the northern end of the island. Discontinuous tracks dominate for vortices approaching the central and southern portion of the Taiwan topography. However, the more intense and rapidly moving vortices moved directly cross over the barrier. Smith and Smith (1995) used a 2-km resolution shallow water model to study the wake formation on the lee side of an island mountain by a drifting vortex. No Coriolis force was included in their experiments. They explored wake formation in terms of the Froude number and the nondimensional

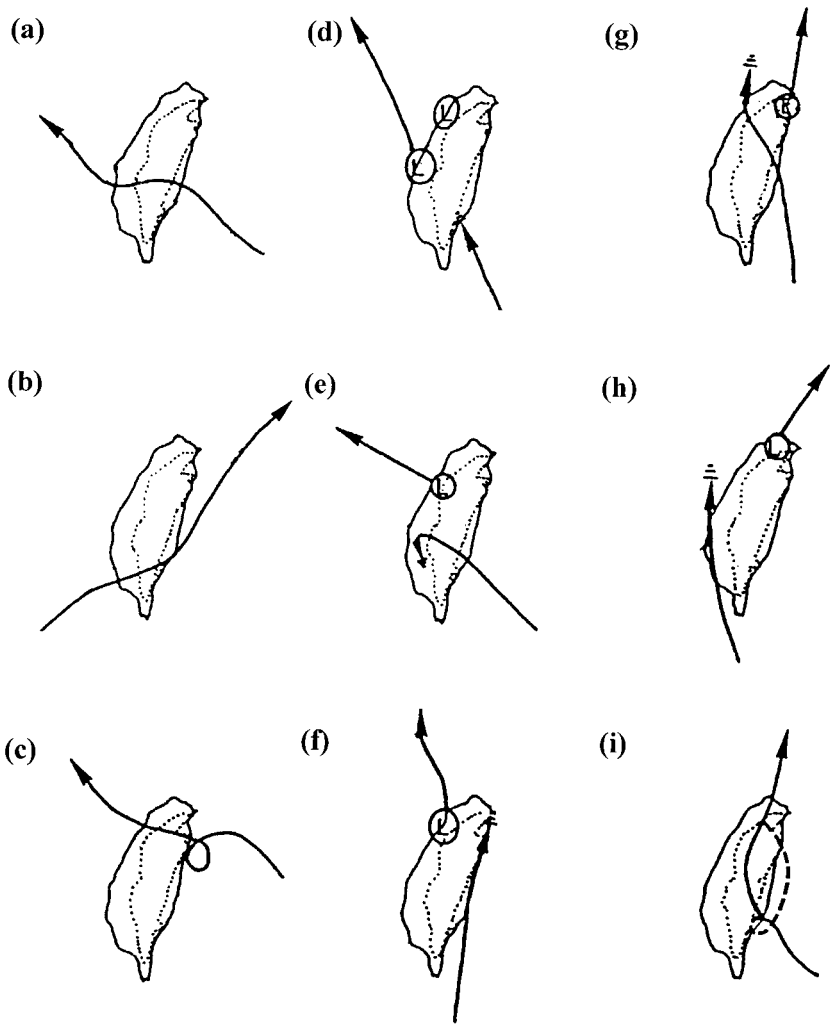

FIG. 1. Typical typhoon tracks across Taiwan that are determined mainly from the surface data available in Taiwan. The tracks are (a) Typhoon Joan 1959, (b) Typhoon Irma 1949, (c) Typhoon Shirley 1960, (d) Typhoon Iris 1955, (e) Typhoon B108 1925, (f) Typhoon Kate 1962, (g) Typhoon B78 1917, (h) Typhoon Bess 1952, and (i) Typhoon Sarah 1989. The symbol "L" indicate the general position of the lee secondary lows. The thick dashed line for Typhoon Sarah (1989) is the track for a strong secondary low that was caused by the chinook wind on the eastern side of central mountain range. The topographic contour of Taiwan is 500 m.

number M, where M is the ratio of mountain height to the shallow water depth. Zehnder (1993) studied the influence of large-scale topography such as the Sierra Madre on barotropic vortex motion with an equatorial β-plane channel model. He found that vortices were deflected toward the imposed gradient of potential vorticity that resulted from the large-scale topography. Zehnder also investigated track deflections as a function of vortex distance from the topography of the Sierra Madre.

The influence of topography on the tropical cyclone strength vortices is very complicated. There are important issues, such as continuous tracks, discontinuous tracks, splitting of upper- and lower-level centers, and the formation of secondary lows, that need to be investigated. One may also wonder if the tracks that are parallel to the topographic contours in the clockwise sense are due to the topographic β effect when the steering flow is weak, as proposed by Carnevale et al. (1991). In this paper, we study one aspect of the basic topographic dynamics and the combination of the local topographic β effect and the global β effect on the hurricane-like vortex tracks and on the coherency of the vortices when there is no mean flow. Both f-plane geometry and spherical geometry calculations are performed. Our simulations suggest the existence of a track mode in which hurricane-like vortices are trapped by the island and follow a clockwise island-circulating

path. Section 2 describes the solution method. The numerical results are presented in section 3, and the concluding remarks are given in section 4.

2. Solution methods

We use both the double periodic f-plane shallow-water model and the global shallow-water model in the study. The shallow-water model can be written as

$$\frac{\partial \zeta}{\partial t} = \alpha(-G, -F), \tag{2.1a}$$

$$\frac{\partial \delta}{\partial t} = \alpha(F, -G) - \nabla^2(I + gh'), \tag{2.1b}$$

$$\frac{\partial h'}{\partial t} = \alpha(-u^*(h' - h_s), -v^*(h' - h_s)) - H\delta. \tag{2.1c}$$

For the global shallow-water model we define the operator α as

$$\alpha(A, B) = \frac{1}{(1 - \mu^2)}\frac{\partial A}{\partial \lambda} + \frac{\partial B}{\partial \mu}, \tag{2.2}$$

and the nonlinear terms as

$$G = U(\zeta + f), \tag{2.3a}$$

$$F = V(\zeta + f), \quad \text{and} \tag{2.3b}$$

$$I = \frac{U^2 + V^2}{2}\frac{a^2}{\cos^2\phi}. \tag{2.3c}$$

For the f-plane shallow-water model we define the operator α as

$$\alpha(A, B) = \frac{\partial A}{\partial x} + \frac{\partial B}{\partial y}, \tag{2.4}$$

and the nonlinear terms as

$$G = u(\zeta + f_0), \tag{2.5a}$$

$$F = v(\zeta + f_0), \quad \text{and} \tag{2.5b}$$

$$I = \frac{u^2 + v^2}{2}. \tag{2.5c}$$

Here, u and v are the zonal and meridional components of velocity, a is the radius of the earth, λ is the longitude, ϕ is the latitude, $\mu = \sin\phi$ is the sine of the latitude, $U = u\cos\phi/a$, $V = v\cos\phi/a$, ζ is the relative vorticity, δ is the divergence, h is the fluid depth, H is the mean equivalent depth, $h' = h - H$, h_s is the topography, f is the Coriolis parameter, and f_0 is the Coriolis parameter for the f plane. In addition, in Eq. (2.1c), we have $u^* = U$ and $v^* = v$ for the global shallow-water model and $u^* = u$ and $v^* = v$ for the f-plane shallow-water model.

The numerical method used in the global model integration is based on the spherical harmonic spectral method in space and the fourth-order Runge–Kutta method in time. Both T96 and T192 resolutions are used for the numerical experiments. The equivalent grid spacings for T96 and T192 resolutions are about 120 and 60 km, respectively. A square domain of 3000 by 3000 km with a grid spacing of 50 km is used for the f-plane experiments. The numerical method is based on the Fourier spectral method in space and the fourth-order Runge–Kutta method in time. Following Smith and Smith (1995), H is set to 5000 m in both models. All the simulations are without the numerical diffusion added to the right-hand side of (2.1). The idealized island topography is given by the function

$$h_s = h_{\max}\exp\left[-\left(\frac{x - x_0}{a_0}\right)^2 - \left(\frac{y - y_0}{b_0}\right)^2\right], \tag{2.6}$$

where (x_0, y_0) is the location of the topographic center, a_0 and b_0 the e-folding widths in the two directions, and $h_{\max}$ the maximum height of the topography. The characteristic topographic slope is determined by the constants $h_{\max}$, a_0, and b_0. The topographic β effect is related only to the slope of the topography. We employ a_0/b_0 ratios of ⅓ or ⅔ for most of our simulations. With these ratios, the orientation of the island topography is similar to the orientation of the island of Taiwan. The only difference between the circular topography ($a_0 = b_0$) and elliptical topography is that the slope in circular topography is isotropic. The topographic slope is smaller along the major axis in the elliptical topography.

The cyclone vortex used in this study has the tangential wind $v(r)$ profile

$$v(r) = v_{\max}\left(\frac{r}{r_{\max}}\right)\exp\left[\frac{1}{b}\left(1 - \left(\frac{r}{r_{\max}}\right)^b\right)\right], \tag{2.7a}$$

and the corresponding vorticity profile

$$\zeta(r) = \frac{2v_{\max}}{r_{\max}}\left[1 - \frac{1}{2}\left(\frac{r}{r_{\max}}\right)^b\right]\exp\left[\frac{1}{b}\left(1 - \left(\frac{r}{r_{\max}}\right)^b\right)\right], \tag{2.7b}$$

where r is the distance to the vortex center, $v_{\max}$ the value of $v(r)$ at the radius of maximum wind $r_{\max}$, and b is a factor that determines the shape of the vortex. Equation (2.7a) has been used previously in many tropical cyclone studies (e.g., DeMaria and Chan 1984). We follow Chan and Williams (1987) by taking b to be 1.0. Once the initial $v(r)$ and $\zeta(r)$ are specified, the initial fluid depth h is computed from the nonlinear balance equation. The initial center of the vortex in the f plane experiments is near the topography. For the calculations with the global shallow-water model, we have designed the experiments so that the vortex impinges on the topography near the southern tip of the island from the southeast of the island. Since the β drift of the vortex without a mean flow is northwestward, the impinging angles of the vortex to the island are not very different in our experiments. Table 1 and Table 2 summarize the relevant parameters for the f plane experiments and spherical experiments, respectively.

TABLE 1. *f*-plane experiments.

Figure		a_0 (km)	b_0 (km)	h_{max} (m)	V_{max} (m s^{-1})	r_{max} (km)
2		200	300	3500	20	100
3	a	400	600	3500	10	100
	b				20	
	c				30	
	d				40	
4	a	400	600	1500	20	100
	b			2500		
	c			3500		
	d			4500		
5	a	200	300	3500	20	100
	b					200
	c					300
	d					400

3. Numerical results

a. f-plane experiments

Figure 2 shows the potential vorticity and wind vectors at hour 20, 40, 60, and 80 on an f plane. The island topography parameters are $h_{max} = 3500$ m, $a_0 = 200$ km, and $b_0 = 300$ km. The vortex parameters are $v_{max} = 20$ m s^{-1} and $r_{max} = 100$ km. The normalized potential vorticity $[(H/f_0)(\zeta + f_0)/h]$ contours start at 0 and increment by 5. The maximum vector is 20 m s^{-1}. The topography contours in all the f plane experiments start at 1000 m and increment by 1000 m. Figure 2 illustrates an island-circulating vortex track that is very similar to the water tank experiment reported by Carnevale et al. (1991). Carnevale et al. (1991) studied propagation of barotropic vortices over topography in a rotating tank. They reported that a small-scale cyclonic vortex on a relatively broad hill tends to climb toward the top in an anticyclonic spiral around the peak. The idea is that when the equivalent potential vorticity is positive, as with the hill, the vortex Rossby waves propagate to the northwest of the local potential vorticity gradient (Adem 1956; McWilliams and Flierl 1979; Chan and Williams 1987; among others). This ''local northwest'' propagation rule implies that a cyclone will spiral toward the top of the hill in an anticyclonic sense. The anticylonic spiral, however, cannot apply when the scale of the vortex is much larger than that of the hill. In laboratory experiments performed at National Taiwan University, Chu et al. (1998, Fig. 7) also reported Rankine-like vortices orbiting a circular hill in a clockwise direction in a rotating tank.

Figure 3 shows the sensitivity of the track to the vortex intensity v_{max} for the f-plane experiments. The topographic parameters are $a_0 = 400$ km, $b_0 = 600$ km, and $h_{max} = 3500$ m. The vortex scale parameter is $r_{max} = 100$ km, and v_{max} is 10, 20, 30, and 40 m s^{-1} in (a), (b), (c), and (d), respectively. The black dot represents the center position (potential vorticity maximum) of the vortex. The vortex initial position is indicated by the ''×'' symbol. The time interval between adjacent black dots is 12 h. The total integration time is 120 h. Figure 3 demonstrates the insensitivity of the trapping of the hurricane-like vortices to v_{max}. Figure 4 is similar to Fig. 3 and shows the sensitivity of the track to the h_{max} parameter. The topographic parameters are $a_0 = 400$ km

TABLE 2. Sphere-plane experiments.

Figure		a_0 (km)	b_0 (km)	h_{max} (m)	V_{max} (m s^{-1})	r_{max} (km)	ϕ_0
6	a	100	150	4500	20	100	45
	b	50		4500			
	c	100		2500			
	d	50		2500			
7	a	600	600	2500	20	100	45
	b		500				
	c		400				
	d		300				
8	a	300	600	2500	20	300	15
	b						25
	c						35
	d						45
9	a	300	600	2500	10	300	25
	b				20		
	c				30		
	d				40		
10	a	300	600	1000	20	300	25
	b			2000			
	c			3000			
	d			4500			
11	a	300	600	2500	20	300	25
	b					400	
	c					500	
	d					600	
12 (initial position of vortex is 3° north)		300	600	2500	20	300	25
					40	300	
					20	600	

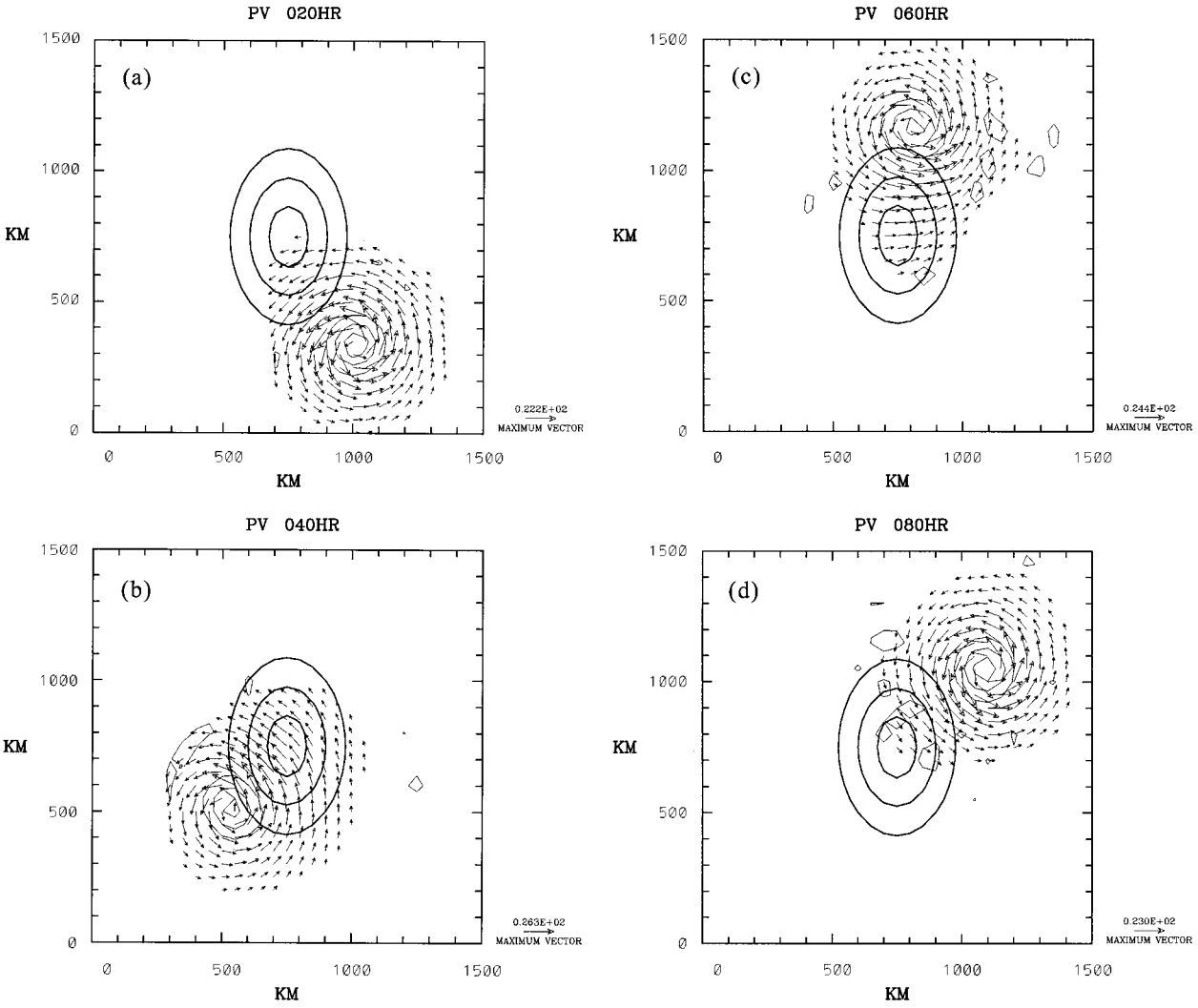

FIG. 2. Potential vorticity and wind vectors at hour 20, 40, 60, and 80 with 50-km grid spacing on a 15° north latitude f-plane experiment. The island topography parameters are $h_{max} = 3500$ m, $a_0 = 200$ km, and $b_0 = 300$ km. The vortex parameters are $v_{max} = 20$ m s^{-1} and $r_{max} = 100$ km. The normalized potential vorticity contours start at 0 and increment by 5. The maximum vector is 22.2, 26.3, 24.4, and 22 m s^{-1} for (a), (b), (c), and (d), respectively. The topography contours start at 1000 m and increment by 1000 m.

and $b_0 = 600$ km. The vortex parameters are $r_{max} = 100$ km and $v_{max} = 20$ m s^{-1}. The value of h_{max} is 1500, 2500, 3500, and 4500 m in (a), (b), (c), and (d), respectively. Figure 4 indicates that vortex trapping is significant when h_{max} is increased. Figure 5 is similar to Fig. 3 and shows the sensitivity of the track to the vortex scale r_{max}. The topographic parameters are $a_0 = 200$ km, $b_0 = 300$ km, and $h_{max} = 3500$ m. The vortex parameter is $v_{max} = 20$ m s^{-1}. The value of r_{max} is 100, 200, 300, and 400 km in (a), (b), (c), and (d), respectively. In the case of Fig. 5d, we have $r_{max} > a_0$, and the trapping is not as significant as in Fig. 5a. In agreement with Carnevale et al. (1991), Fig. 5 implies that the topographic scale needs to be larger than the vortex radius of maximum wind for the trapping to be significant. The scale for the trapping means that the maximum wind of the vortex has to cross the slope of the topography for the topographic β effect to be important.

Although the trapping of the hurricane-like vortices is insensitive to v_{max}, the drift speed along the clockwise path is larger for the vortex with a larger maximum wind. The speed estimated from Fig. 3 is approximately 6.2, 9.9, 12.4, and 16.1 m s^{-1} in (a), (b), (c), and (d), respectively. It appears that the drift speed is proportional to the square root of v_{max}. This is in agreement with the scaling law for nondivergent tropical cyclone motion on the β plane (Smith 1993; Smith et al. 1997). The drift speed in Fig. 4 is estimated to be 5.4, 6.2, 9.8, and 12.5 m s^{-1} in (a), (b), (c), and (d), respectively. The drift speed in Fig. 4 is proportional to $\sqrt{\beta_e}$, which shows general agreement with the Smith scaling law. The topographic β effect is defined as

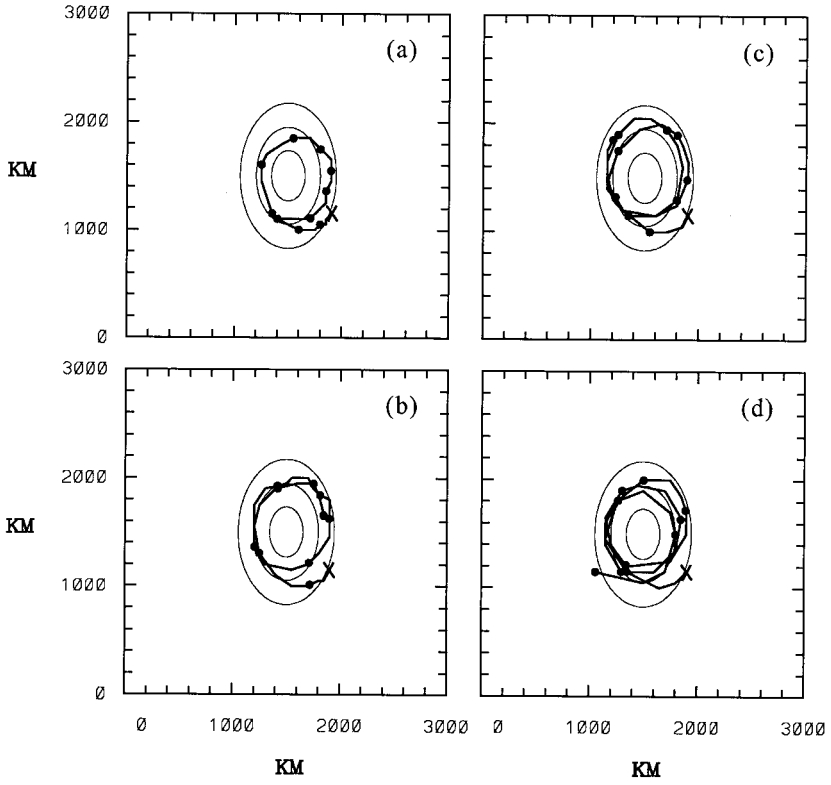

FIG. 3. The sensitivity of the track with respect to the vortex intensity v_{max} for the f plane experiments. The topographic parameters are $a_0 = 400$ km, $b_0 = 600$ km, and $h_{max} = 3500$ m. The vortex scale parameter is $r_{max} = 100$ km, and v_{max} is 10, 20, 30, and 40 m s^{-1} in (a), (b), (c), and (d), respectively. The black dot represents the center position (potential vorticity maximum) of the vortex. The vortex initial position is indicated by the ''×'' symbol. The topography contours start at 1000 m and increment by 1000 m. The time interval between adjacent black dots is 12 h. The total integration time is 120 h.

$$\beta_e = \frac{f}{H}\frac{h_{\max}}{a_0},$$

where we have used the *e*-folding distance of the topography in the east–west direction for the terrain slope calculation. The estimated drift speed in Fig. 5 is approximately 5.4, 5.4, 5.4, and 3.7 m s^{-1} in (a), (b), (c), and (d), respectively. The drift speeds in Fig. 5, however, are not in agreement with the Smith scaling law. This probably has to do with the portion of the topography that is felt by the vortex in Fig. 5; this varies as we change our r_{max} parameter. It appears that the application of the Smith scaling law to our calculation is quite sensitive to the degree that the local β_e effect is felt by the vortex. The Smith scaling law applied to our discussion indicates that $v_d \sim \sqrt{\beta_e v_{\max}}$. The dynamics of the Smith scaling law indicate that the drift speed v_d is proportional to the asymmetric vorticity ζ_a. The ζ_a results from the local vorticity advection (order of $\beta_e v_{\max}$) and is destroyed by the drift of the vortex. Thus, we have

$$v_d \sim \zeta_a \sim \frac{\beta_e v_{\max}}{v_d}, \quad \text{and} \quad v_d \sim \sqrt{\beta_e v_{\max}}.$$

Note that the parameter v_{max} that is used in the Smith scaling law only describes the inner part of the vortex wind profile. According to Fiorino and Elsberry (1989), the strength and radius of maximum wind have little influence on the drift speed when a variety of vortex shapes are considered. It is the outer parts of the vortex that act with β to create a steering current to advect the inner vortex. Thus, the scaling law is valid for vortices with specific wind profiles.

With the drift speed related to the ''local northwestward'' propagation, it is natural to ask whether the vortex will reach the top of the island and remain locked there. We have not observed such phenomena in our simulations. Carnevale et al. (1991) also did not find this behavior for vortex motion on a conical hill. They pointed out that the vortex flow over the peak would cause the development of an anticyclonic circulation over the peak. This would block the movement toward the peak and cause the vortex to move around the peak in a clockwise direction, as they observed. From another point view the vortex does not climb to the top because the length scale of horizontal gradient of topography approaches zero near the top. Thus, a vortex cannot continue its drift toward the peak of the island.

We have also performed linear calculations for our

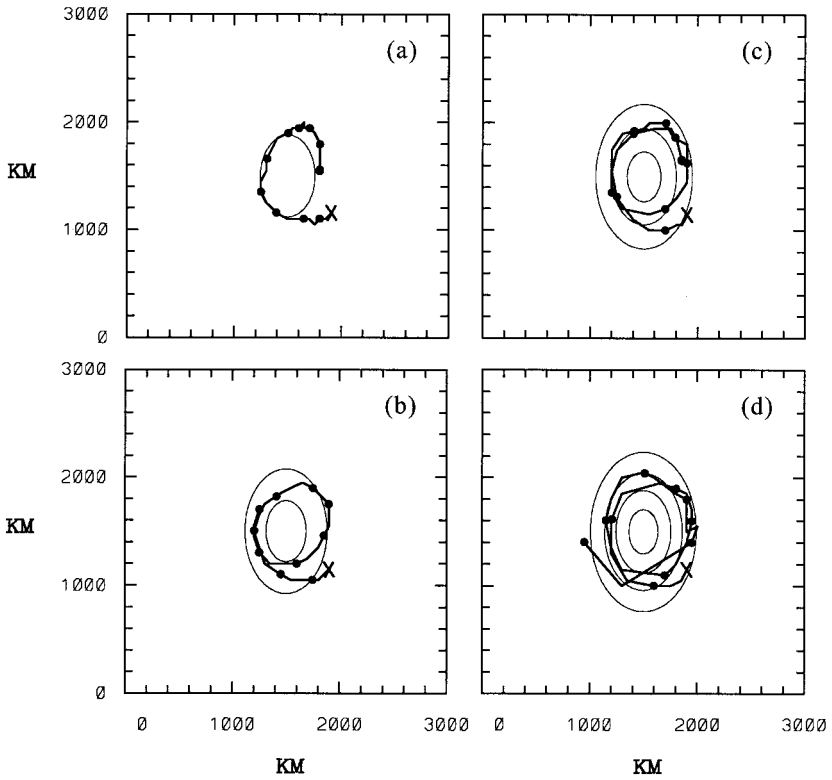

FIG. 4. Similar to Fig. 3 except for the sensitivity of the track with respect to the h_{max} parameter. The topographic parameters are $a_0 = 400$ km, and $b_0 = 600$ km. The vortex parameters are $r_{max} = 100$ km and $v_{max} = 20$ m s^{-1}. The h_{max} is 1500, 2500, 3500, and 4500 m in (a), (b), (c), and (d), respectively.

f-plane experiments. Our linear calculations indicate a slower drift speed circulating the topography (not shown here). The slower speed in the linear case may be due to dispersion effects. It is the nonlinear effect that holds the vortex together and protects the vortex from strong dispersion in the island-circulating path. The dynamical basis for the dispersion-resistant properties in a barotropic vortex can be discussed in terms of the so-called β Rossby number (McWilliams and Flierl 1979; Sutyrin and Flierl 1994). The β Rossby number is the ratio of the nonlinear terms in the vorticity equation to the linear vortex Rossby wave dispersion term. The β Rossby number in our application can be defined as

$$R_\beta = \frac{v_{max}}{\beta_e r_{max}^2}.$$

When this dimensionless parameter drops below unity, a stronger β_e dispersion and energy radiation from the vortex is expected. When the number is of order of unity, the nonlinear effect is important, and the vortex can hold itself against the dispersion. With the r_{max} of the order 100 km in our specified vortex, it requires a v_{max} of a few meters per second for the nonlinear effect to be important. The nonlinear dynamics are thus important for tropical cyclone strength vortices. The nonlinear dynamics of ''asymmetry damping'' (to make the vortex remain circular) were also studied by Carr and Williams (1989) with the bounded Rankine vortex with zero basic state vorticity gradient. Smith and Montgomery (1995) generalized Carr and Williams' 1989 solution to the case of unbounded Rankine flow. On the other hand, Dritschel (1998) and Kuo et al. (1999) suggested that the nonlinear dynamics hold all the vortex Rossby waves moving in phase at the same phase speed and maintain the elliptical vortices from dispersion. The dynamics of barotropic vortex Rossby waves that propagate both radially and azimuthally on the radially continuous waveguide of the vortex vorticity gradient was thoroughly studied by Montgomery and Kallenbach (1997).

b. Sphere experiments

The tracks for the experiments on the sphere with a T192 resolution global shallow-water model are presented in Fig. 6. The topography contours in all the global shallow-water model experiments start at 500 m and increment by 500 m. The vortex parameters are $r_{max} = 100$ km and $v_{max} = 20$ m s^{-1}. The topography is centered at 45° north latitude, and (a) $a_0 = 100$ km, $b_0 = 150$ km, $h_{max} = 4500$ m; (b) $a_0 = 50$ km, $b_0 = 150$ km, $h_{max} = 4500$ m; (c) $a_0 = 100$ km, $b_0 = 150$ km, $h_{max} = 2500$ m; and (d) $a_0 = 50$ km, $b_0 = 150$ km, h_{max}

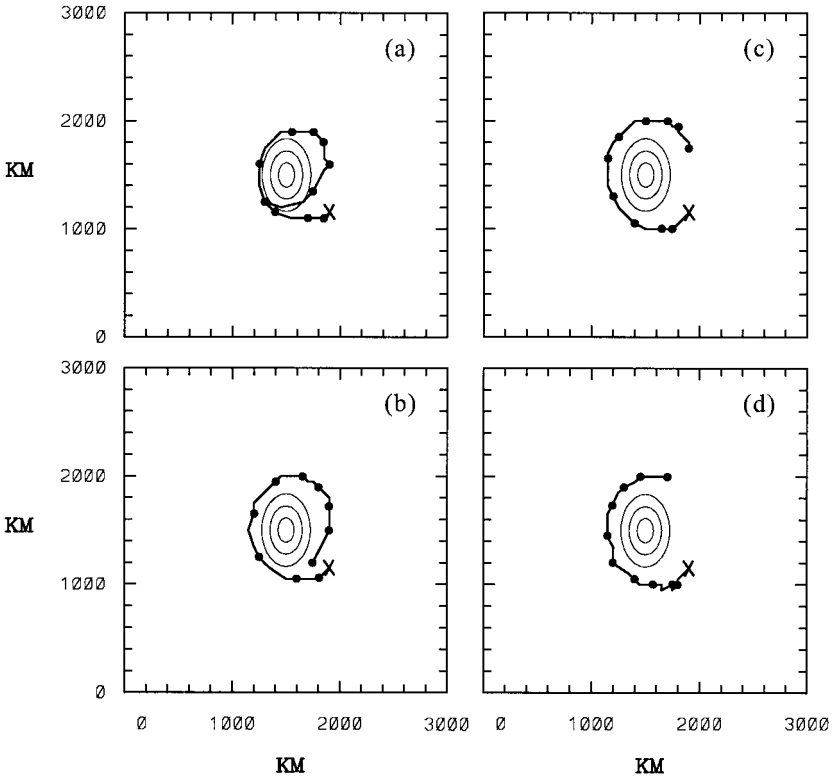

FIG. 5. Similar to Fig. 3 except for the sensitivity of the track with respect to the vortex scale r_{max}. The topographic parameters are $a_0 = 200$ km, $b_0 = 300$ km, and $h_{max} = 3500$ m. The vortex parameter is $v_{max} = 20$ m s^{-1}. The r_{max} is 100, 200, 300, and 400 km in (a), (b), (c), and (d), respectively.

$= 2500$ m. The black dot represents the center position (potential vorticity maximum) of the vortex. The time interval between adjacent black dots is 24 h. The vortex initial position is indicated by the $\times$ symbol. The total integration time is 216 h. Comparing Fig. 6a with the f plane results, we see that the island-circulating path may also occur in the presence of a planetary vorticity gradient. Although the topographic slope is larger in the case of Fig. 6b, the vortex still breaks away from the island after a partial clockwise island-circulating track. The vortices in Figs. 6c and 6d break away from the island after some clockwise influence. It is clear from Fig. 6 that a higher mountain favors the existence of an island-circulating track. The presence of the global β effect, contrary to the local β_e effect, tends to break the vortex away from the topography.

To understand the dynamics of vortex trapping on the sphere, we have performed extensive T96 experiments with larger topographic parameters a_0, b_0, and a larger r_{max}. The larger parameter range is chosen to allow extensive experiments with less cost and to avoid resolution problems. The scale parameters are larger than would be expected in real tropical cyclones, but a comparison of the T96 and T192 solutions shows that the fundamental dynamics are not altered by using larger scales. The following experiments are performed with the T96 resolution. Note that the track dynamics due to the variation of b_0 are not equivalent to the track dynamics due to the variation of a_0 on the sphere. Figure 7 shows the sensitivity of the track to the topographic parameter b_0. The topography is at 25° latitude and $h_{max} = 2500$ m. The topographic e-folding distances are (a) $a_0 = 600$ km, $b_0 = 600$ km, (b) $a_0 = 600$ km, $b_0 = 500$ km, (c) $a_0 = 600$ km, $b_0 = 400$ km, and (d) $a_0 = 600$ km, $b_0 = 300$ km. Figure 7 indicates that the vortex trapping is not as sensitive to the parameter b_0 as to the parameter a_0. Similar to Fig. 7, Fig. 8 shows the sensitivity of the track to the latitude of the island. The topographic parameters are $a_0 = 300$ km, $b_0 = 600$ km, and $h_{max} = 2500$ m. The vortex parameters are $r_{max} = 300$ km and $v_{max} = 20$ m s^{-1}. The latitude of the island is 15°, 25°, 35°, and 45° in (a), (b), (c), and (d), respectively. Figure 8 shows that a higher latitude island favors the clockwise island-circulating track. Moreover, the drift speed in the island-circulating track is slower in the low latitude case. This may be due in part to the fact that the Coriolis force is larger at higher latitudes in addition to the slower β-induced speed in high latitudes. Due to the complication of the β effect, the drift speed does not appear to be in agreement with the Smith scaling law.

Figure 9 shows the sensitivity of the track to the

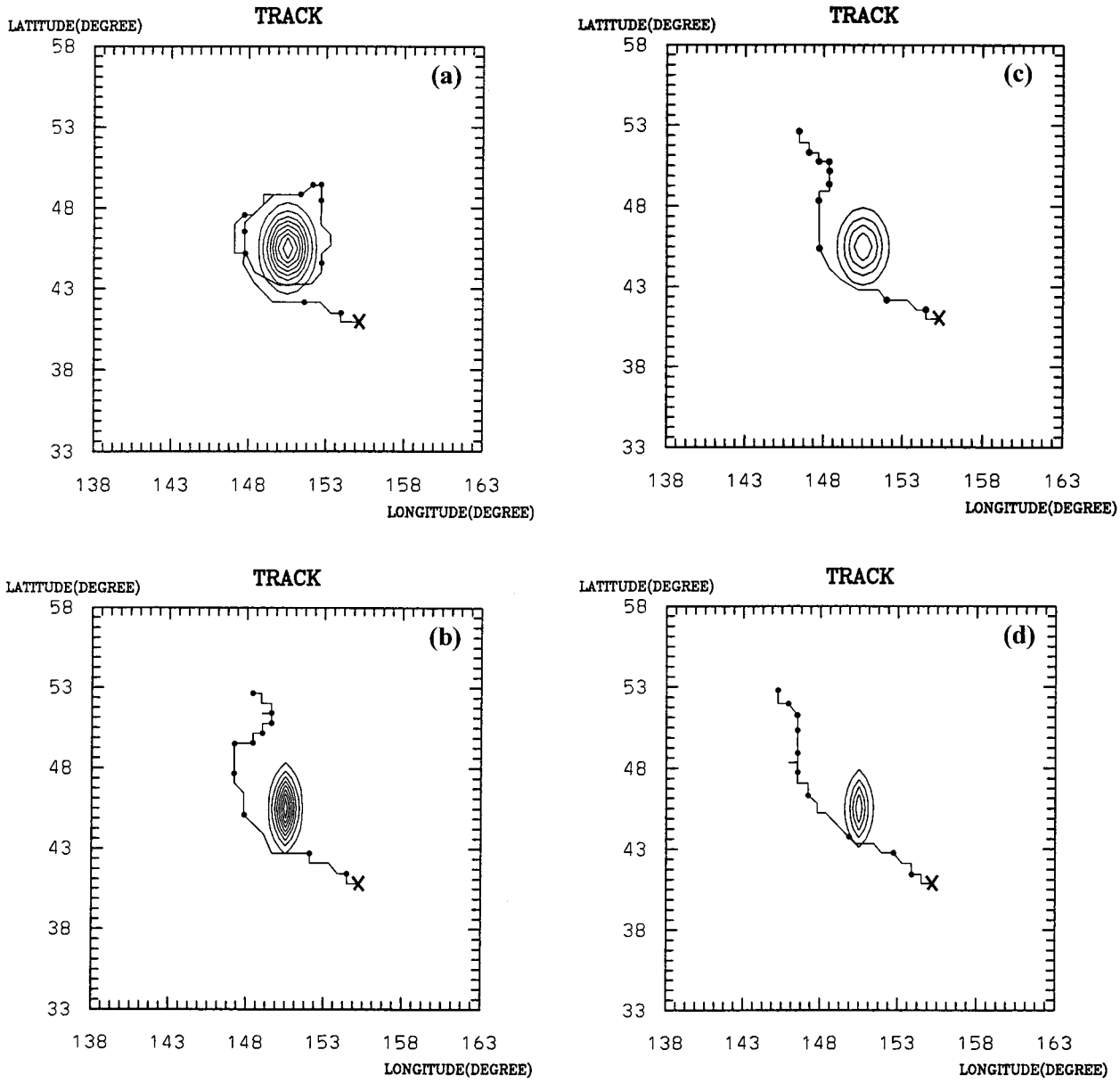

FIG. 6. The track for the experiments on the sphere with global shallow-water model. The vortex parameters are $r_{max} = 100$ km and $v_{max} = 20$ m s^{-1}. The topography is centered at 45° north latitude, and (a) $a_0 = 100$ km, $b_0 = 150$ km, $h_{max} = 4500$ m; (b) $a_0 = 50$ km, $b_0 = 150$ km, $h_{max} = 4500$ m; (c) $a_0 = 100$ km, $b_0 = 150$ km, $h_{max} = 2500$ m; and (d) $a_0 = 50$ km, $b_0 = 150$ km, $h_{max} = 2500$ m. The topography contours start at 500 m and increment by 500 m. The black dot represents the center position (potential vorticity maximum) of the vortex. The time interval between adjacent black dots is 24 h. The vortex initial position is indicated by the "×" symbol. The total integration time is 216 h.

vortex intensity v_{max} for the island centered at 25° latitude. The topographic parameters are $a_0 = 300$ km, $b_0 = 600$ km, and $h_{max} = 2500$ m. The vortex scale parameter is $r_{max} = 300$ km. The v_{max} is 10, 20, 30, and 40 m s^{-1} in (a), (b), (c), and (d), respectively. As discussed in Chan and Williams (1987) and Smith et al. (1997), the β-induced vortex motion speed (which tends to break the vortex from the topography) increases with increasing v_{max}. It appears that the effect of the mountain also increases with v_{max} so that the net effect would be about the same on the vortex motion. Thus, the trapping of the vortices is not sensitive to the v_{max} of the hurricane-strength vortex.

The sensitivity of the track with respect to h_{max} for the island centered at 25° latitude is shown in Fig. 10. The topographic parameters are $a_0 = 300$ km and $b_0 = 600$ km. The vortex parameters are $r_{max} = 300$ km and $v_{max} = 20$ m s^{-1}. The value of h_{max} is 1000, 2000, 3000, and 4500 m in (a), (b), (c), and (d), respectively. Figure 10 suggests that higher mountains are more favorable

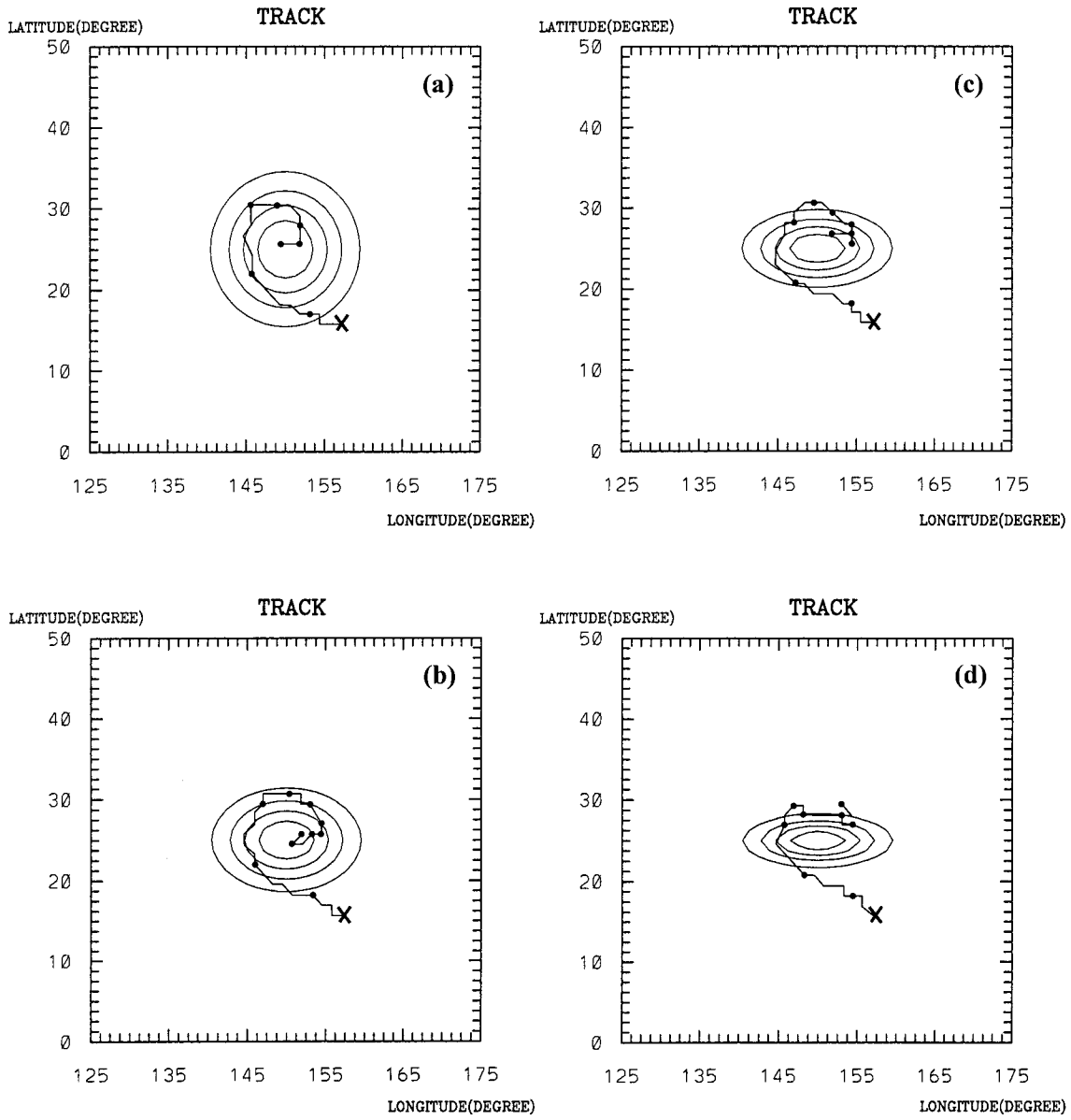

FIG. 7. Similar to Fig. 6 except for the sensitivity of the track with respect to the topographic parameter b_0. The topography is at 25° north latitude and h_{max} = 2500 m. The topographic e-folding distance is (a) a_0 = 600 km, b_0 = 600 km; (b) a_0 = 600 km, b_0 = 500 km; (c) a_0 = 600 km, b_0 = 400 km; and (d) a_0 = 600 km, b_0 = 300 km, respectively.

for island-circulating tracks. Figure 11 shows the sensitivity of the track to the vortex scale r_{max} for the island centered at 25° latitude. The topographic parameters are a_0 = 300 km, b_0 = 600 km, and h_{max} = 2500 m. The vortex parameter is v_{max} = 20 m s^{-1}. The value of r_{max} is 300, 400, 500, and 600 km in (a), (b), (c), and (d), respectively. We observed from Fig. 11 that the vortices with smaller radii of maximum wind are more likely to follow the island-circulating track. For vortices with a comparable ratio of r_{max} to a_0, we see trapping in the f plane runs but no effect on the sphere.

We have so far carried out our spherical experiments with the impinging position of the vortex always to the southeast of the island. Figure 12 is the same as Figs. 9b, 9d, and 11d except that the initial position of the vortex is displaced 3° to the north. By comparing Figs. 12a and 12b with Figs. 9b and 9d, we find that the general properties of vortex trapping for small vortices (r_{max} = 300 km) are similar except for some details in position. By comparing Fig. 12c with Fig. 11d, we find that the track of a larger vortex (r_{max} = 600) is quite chaotic in the sense that a slight change in the initial position (i.e., close to a $3\Delta x$ difference in our experiments) will result in a drastically different track. Figure 12 indicates that the sensitivity of the impinging position of the vortex on the topography on the sphere experi-

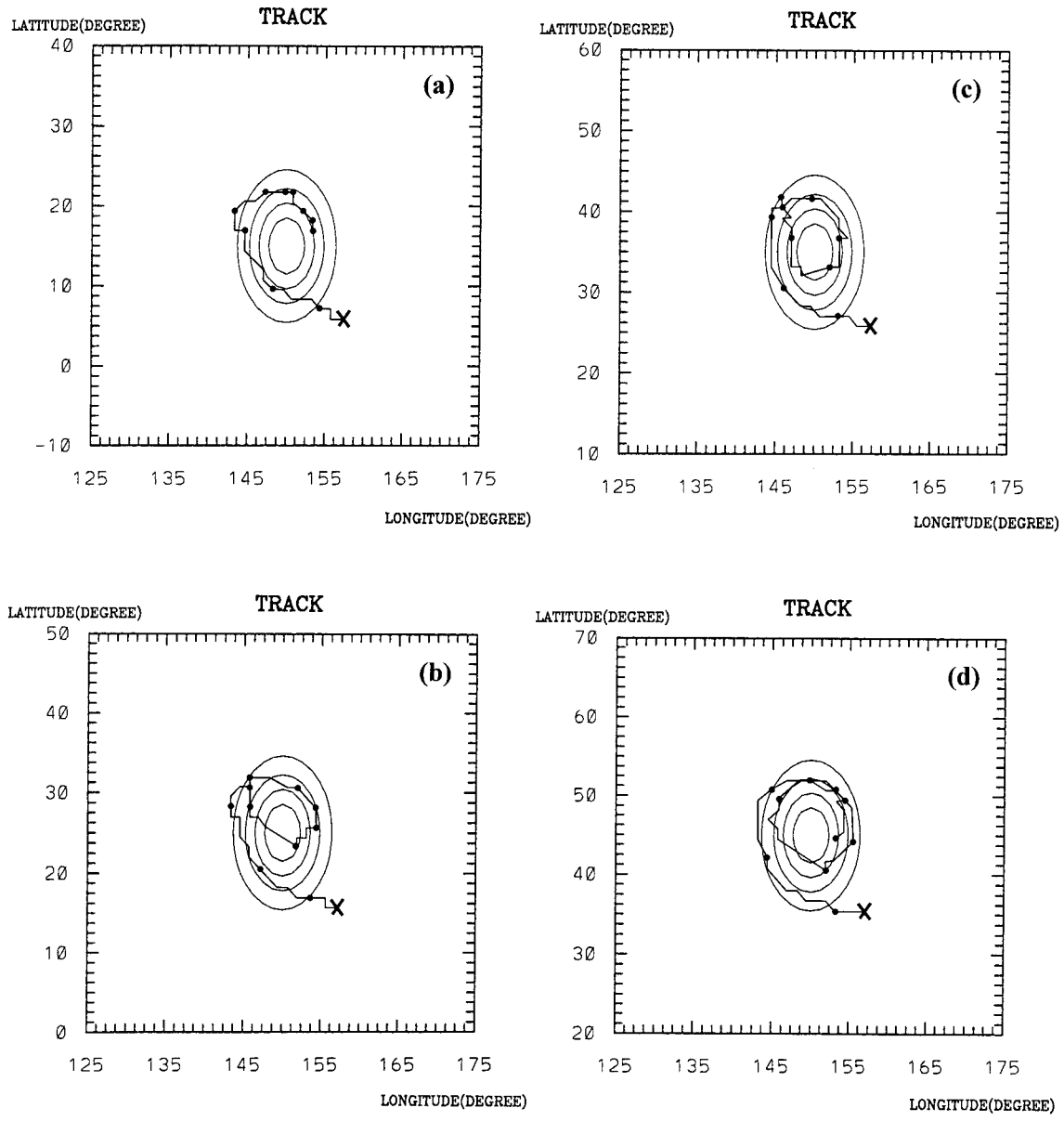

FIG. 8. Similar to Fig. 6 except for the sensitivity of the track with respect to the latitude of the island. The topographic parameters are $a_0 = 300$ km, $b_0 = 600$ km, and $h_{max} = 2500$ m. The vortex parameters are $r_{max} = 300$ km and $v_{max} = 20$ m s^{-1}. The latitude of the island is 15°, 25°, 35°, and 45° north in (a), (b), (c), and (d), respectively.

ments. This is quite different from our f-plane experiments, which show that the trapping is not sensitive to the impinging position. This sensitivity and the bifurcation point for the trapped versus untrapped vortices should be studied with a much higher resolution model.

We have summarized all the T96 experiments in a two-dimensional parameter space. The abscissa in Fig. 13 is the nondimensional parameter β/β_e, and the ordinate is a_0/r_{max}, the ratio of the horizontal width of the topography in east–west direction to the vortex scale in terms of r_{max}. The parameters are chosen on the ground that the island-circulating track is most likely due to the topographic β-drift effect. The parameter β/β_e measures the ratio of the two β-drift effects. The circulating and noncirculating cases are separated by examining the track and the end position of the vortex. Figure 13 suggests that the circulating mode is favored when $a_0/r_{max} \geq 1.7\beta/\beta_e + 0.5$. In general, the trapping and clockwise circulating path in the presence of a planetary vorticity gradient will occur if the scale of the topography is greater than the vortex radius of maximum wind and if the planetary β parameter is less than the topographic β parameter. The β_e effect is to trap the vortex in the vicinity of topography and to produce an island-circulating mode. When β is smaller than β_e, the vortex will be trapped. On the other hand, the vortex scale has to

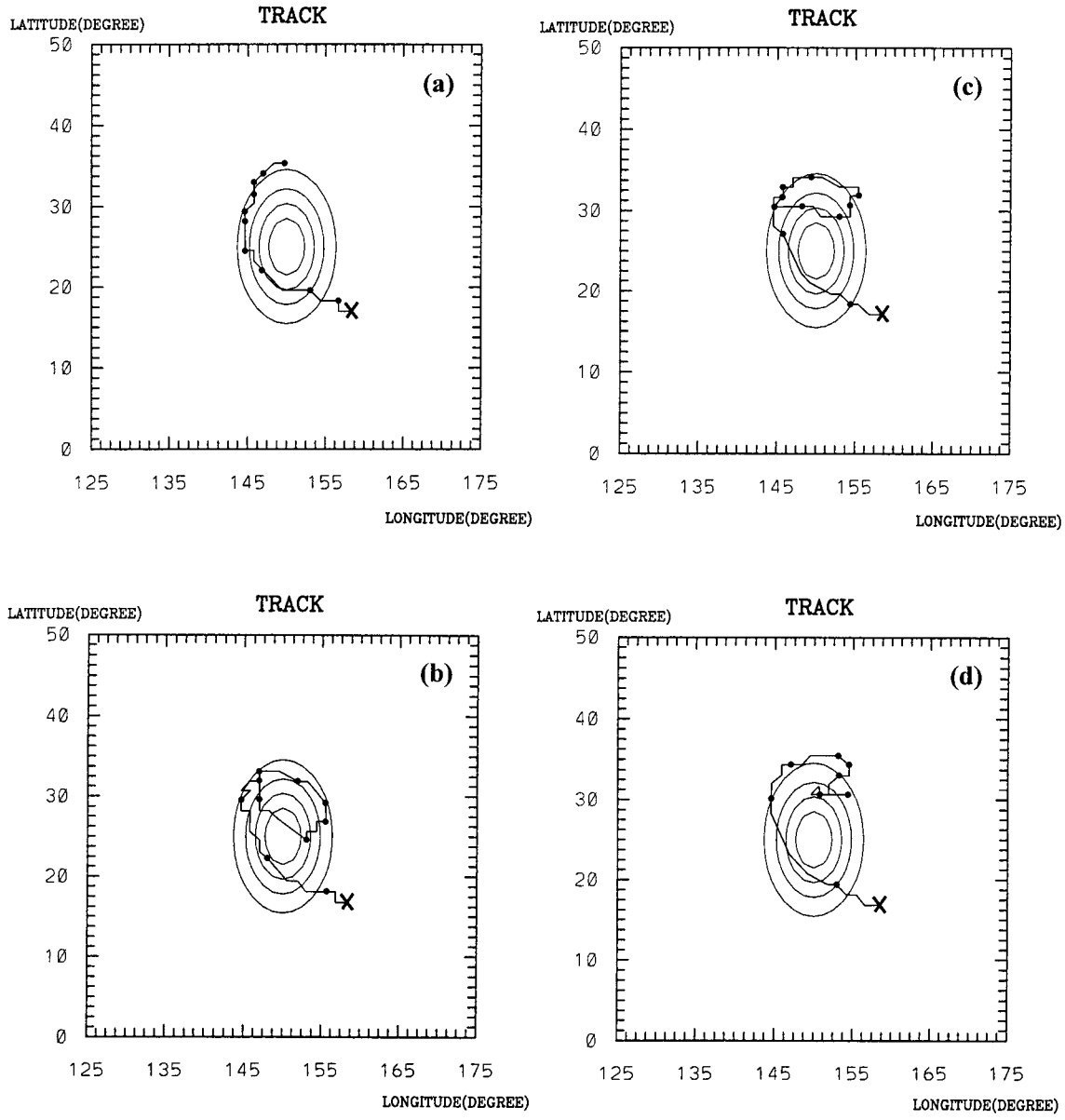

FIG. 9. Similar to Fig. 6 except for the sensitivity of the track with respect to the vortex intensity v_{max} for the island centered at 25° north latitude. The topographic parameters are $a_0 = 300$ km, $b_0 = 600$ km, and $h_{max} = 2500$ m. The vortex scale parameter is $r_{max} = 300$ km. The v_{max} is 10, 20, 30, and 40 m s^{-1} in (a), (b), (c), and (d), respectively.

be comparable to (if not smaller than) the scale of the topography for the vortex to feel the existence of the topography. The vortex trapping is not sensitive to v_{max} which is why the coordinates in Fig. 13 do not depend on v_{max}.

4. Concluding remarks

The nondispersive, clockwise, island-circulating mode of hurricane-like vortices is qualitatively similar to the coastally trapped waves (e.g., Gill 1977) and Kelvin waves that also possess the nondispersive clockwise island-circulating feature. However, the drift speed in our simulations is very different from the linear gravity wave speed $\sqrt{gH}$. Our phenomena involve the propagation of a finite amplitude potential vorticity anomaly, while linear Kelvin waves have zero potential vorticity. The nondispersive, trapping mode is also clearly seen in rigid lid single-layer quasigeostrophic calculations, which do not support Kelvin waves (Carnevale et al. 1988). We have also performed calculations with a different structure parameter $b = 0.25$ in (2.7) and with a shallower equivalent depth. A rich variety of tracks were simulated. The clockwise, island-circulating modes in these simulations were qualitatively similar. With a shallower mean depth, we observed a slower circulating

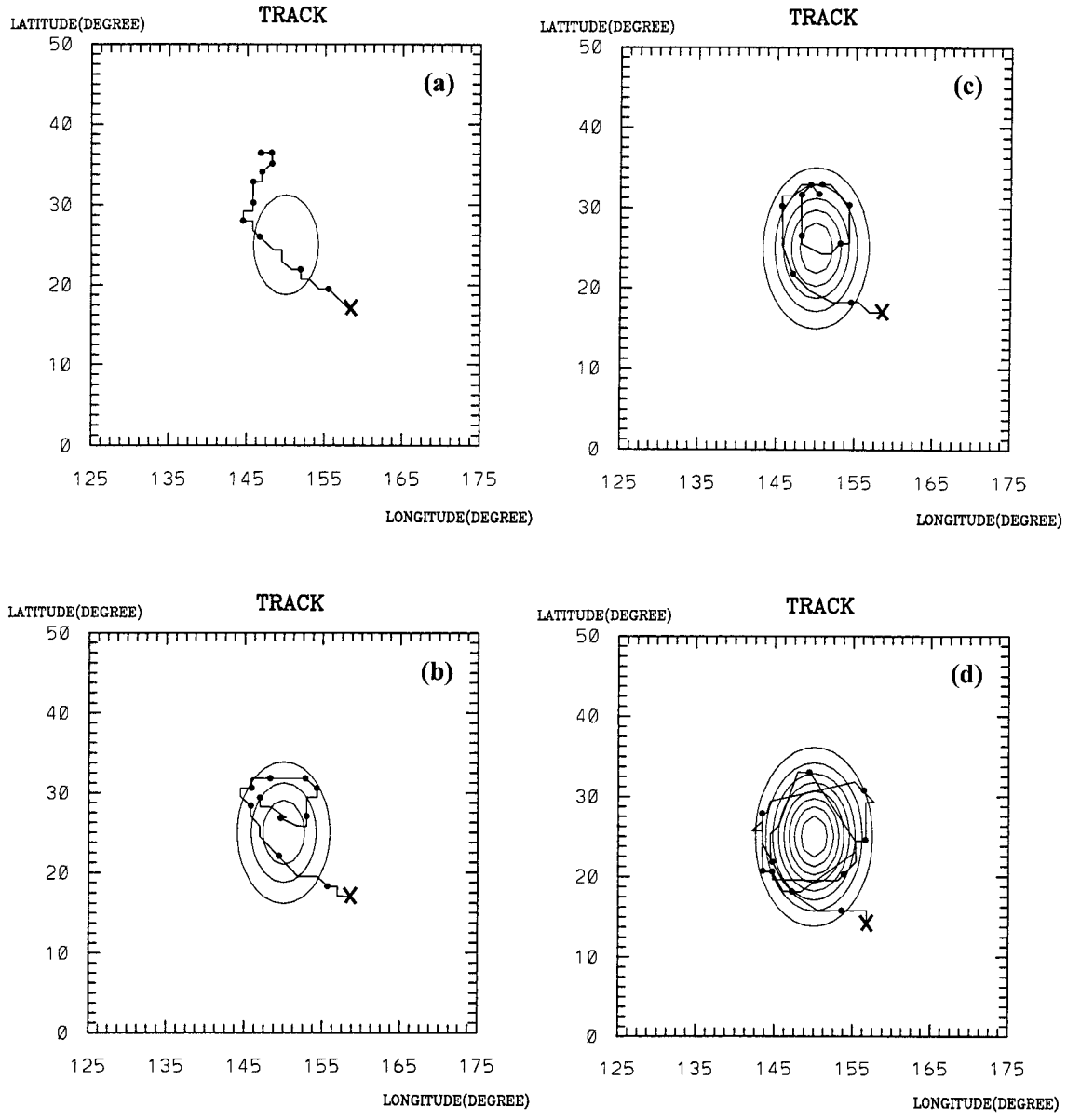

FIG. 10. Similar to Fig. 6 except for the sensitivity of the track with respect to the h_{max} parameter for the island centered at 25° latitude. The topographic parameters are $a_0 = 300$ km and $b_0 = 600$ km. The vortex parameters are $r_{max} = 300$ km and $v_{max} = 20$ m s^{-1}. The h_{max} is 1000, 2000, 3000, and 4500 m in (a), (b), (c), and (d), respectively.

motion, which is consistent with the divergent topographic β-drift effects. A thorough analysis of the divergence effect on the shallow-water model results can be found in Zehnder (1993).

We have observed wake and secondary low formation in some of our calculations with a mountain peak height of 4500 m (i.e., $M = 0.9$). These lows sometimes also followed the island-circulating track and at times merged with the main vortex. The trapping and clockwise circulating path does not seem to be affected by these mesoscale features. A detailed comparison with Smith and Smith (1995) cannot be made due to the inadequate resolution used in our calculations. Recent observations by Doppler on Wheel (Gall et al. 1998; Wurman and Winslow 1998) revealed the existence of intense, small-scale spiral bands for landfall hurricanes. These spiral bands have spatial scales on the order of subkilometer to 10 km and extend through depths of 1 to 5–6 km. It appears that the mesoscale features (horizontal length scale smaller than the terrain scale) associated with typhoon landfall are very complicated, and these multiple scale structures are not well resolved by observations. No attempt has been made to explore the details of mesoscale features of secondary lows in this paper. Rather, the focus has been on the major features in the vortex track in response to the terrain. There are

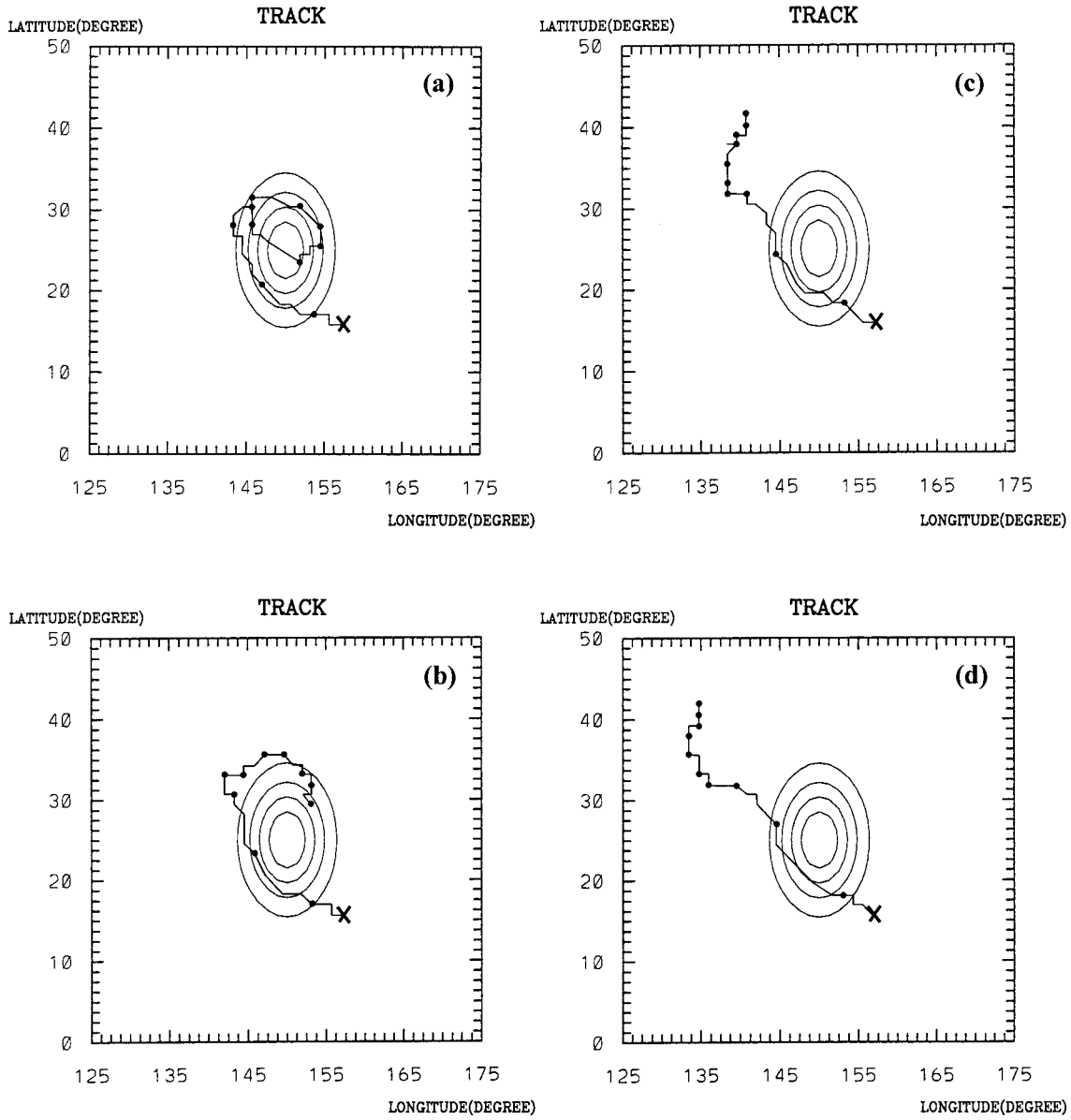

FIG. 11. Similar to Fig. 6 except for the sensitivity of the track with respect to the vortex scale r_{max} for the island centered at 25° latitude. The topographic parameters are $a_0 = 300$ km, $b_0 = 600$ km, and $h_{max} = 2500$ m. The vortex parameter is $v_{max} = 20$ m s^{-1}. The r_{max} is 300, 400, 500, and 600 km in (a), (b), (c), and (d), respectively.

problems, such as the development mechanism of the secondary low, severe downslope winds, boundary layer structure, and frictional drag effects in landfalling hurricanes, that deserve further study.

Zehnder (1993) studied the influence of large-scale topography, such as the Sierra Madre, on barotropic vortex motion with an equatorial β-plane channel model. He found that the motion of vortices is deflected by the large-scale topography. As clearly pictured in his Figs. 5 and 8, a vortex that approaches the topography from the east is accelerated and deflected toward the south, and a vortex initially west of the mountain recurves and moves toward the east. It is clear that our island-circulating mode is consistent with the simulations of Zehnder. Since the spatial scale of the Sierra Madre is much greater than the vortex scale, the deflections produced by the island-circulating mode can be quite significant. In fact, Zehnder argued that the mechanism might be important in forecasting hurricane motion in the eastern north Pacific and the western Gulf of Mexico. A study on the propagation of wintertime synoptic scale low-level circulation features in the vicinity of a mountain range in terms of topographic Rossby waves can be found in Hsu (1987). Hsu argued that the steering effect of topography upon atmospheric circulations is restricted to the lower atmosphere due to

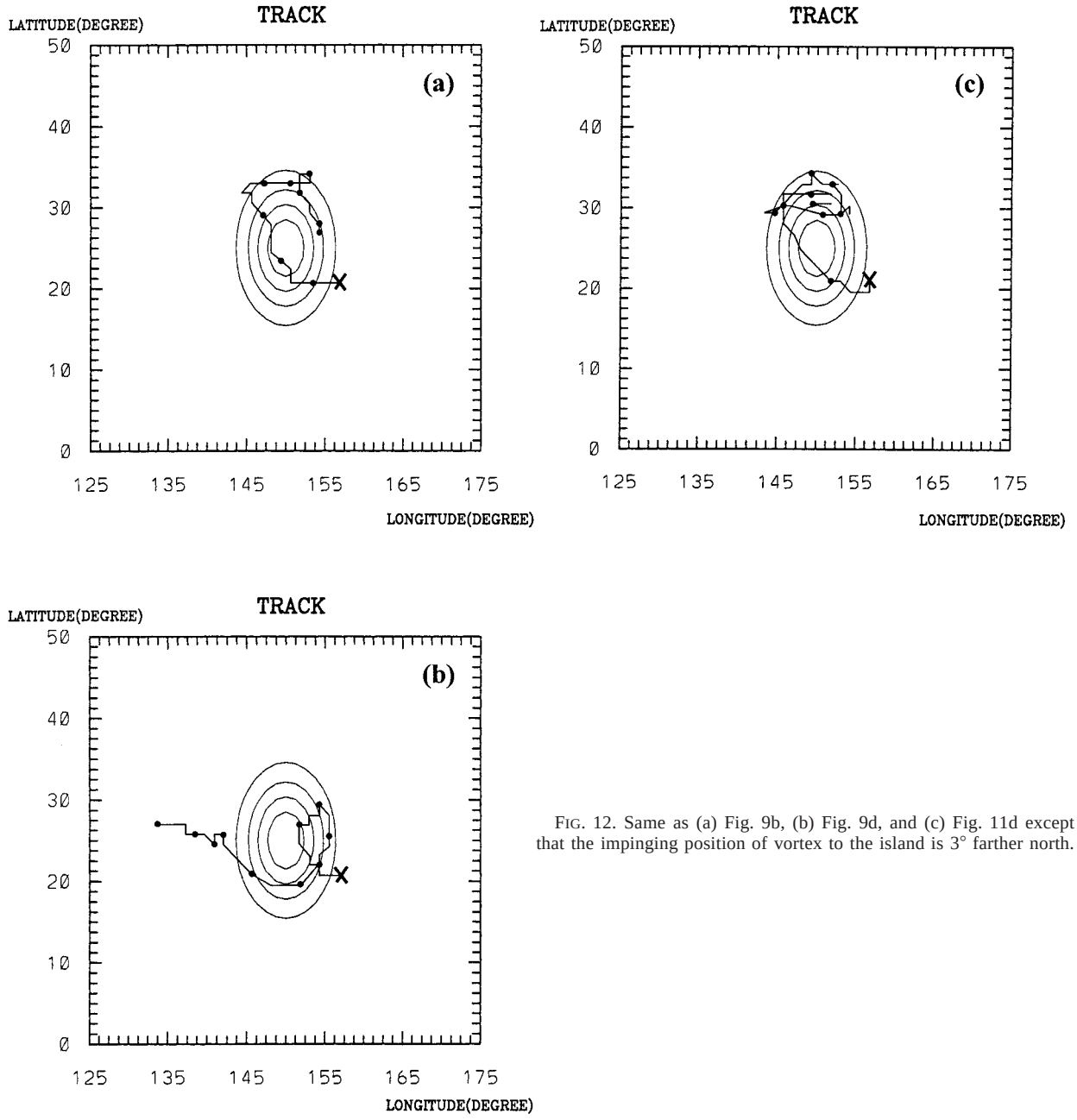

FIG. 12. Same as (a) Fig. 9b, (b) Fig. 9d, and (c) Fig. 11d except that the impinging position of vortex to the island is 3° farther north.

the strong vertical stratification in wintertime. However, the dominant diabatic processes in tropical cyclones can greatly increase the vertical coupling. The topography-induced steering may not be restricted to the lower atmosphere for the hurricane.

Although the calculations contain no mean flow, our discussion can shed some light on the situation when mean flow is present. Let us consider a situation where the mean steering flow does not vary appreciably over the spatial scale of the island. Without the spatial variation of the mean flow, the ''environmental β-drift'' due to the potential vorticity gradient of mean flow is not present. Our results indicate that vortices with smaller radius r_{max} and islands with a higher peak height, with a wider east–west scale and which are at a higher latitude favor vortex trapping into a clockwise, island-circulating track. To be consistent with the results, we need to consider both the scale parameter r_{max}/a_0 and the timescale of vortex crossing the topography by advection. The scale of the vortex must be smaller than the scale of the island for the vortex to be trapped. Similarly, the time it takes the vortex to drift directly across the island topography must be longer than the timescale of the earth's rotation $1/f$. This argument can be written in

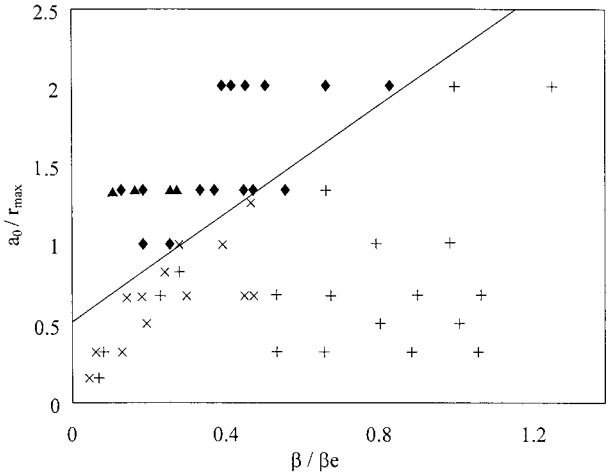

FIG. 13. Summary of numerical experiments with nondimensional parameters. The abscissa is the nondimensional parameter β/β_e, where β_e is the equivalent β effect of the topography. The ordinate is $a_0/r_{\max}$ the ratio of topographic horizontal width to the vortex scale. The island-circulating experiments are indicated by ▲ ($v_{\max}$ = 40 m s^{-1}) and ♦ ($v_{\max}$ = 20 m s^{-1}) symbols. The non-circulating tracks are indicated by × ($v_{\max}$ = 40 m s^{-1}) and + ($v_{\max}$ = 20 m s^{-1}) symbols.

terms of a Rossby number. The topographic deflection is important only when both the appropriate Rossby number and the scale parameter $r_{\max}/a_0$ are smaller than unity. The argument is in agreement with the observations that the more intense and rapidly moving hurricanes moved directly cross over the Taiwan barrier.

With simple dynamical model calculations, our intent is not to underestimate the importance of the moist physics, large-scale steering, and baroclinic effects but rather to isolate the fundamental barotropic aspects of the impact of topography on vortex movement. This study compliments previous work on propagation of barotropic vortices over topography (e.g., Carnevale et al. 1991), and we have extended the track dynamics to include both local topography β_e and global β effects for hurricane-like vortices. When a vortex approaches a low-latitude island like Taiwan, the vortex translation speed and the scale of Taiwan may not be right for the occurrence of a complete island-circulating track. On the other hand, our simulations suggest the possibility of a vortex breaking away from the island after following a partial clockwise island-circulating track for slow-moving small hurricane-like vortices. This partial clockwise island-circulating track can also be seen from time to time in the typhoon tracks cross Taiwan. Examples of such tracks are shown in Fig. 1 for Typhoon Sarah (1989) and Typhoon Bess (1952). The general agreement of the nondispersive local β_e vortex dynamics with the observations, however, may also be coincidental. With the very limited upper-air observations during typhoon landfall, it is difficult to distinguish the β_e effect from the environmental steering effect.

Our results can also be interpreted in terms of potential vorticity conservation. We can view the topography as a fixed positive potential vorticity anomaly, which comes only from the mass field. Our vortex-trapping problem can then be interpreted as an interaction of a time-varying potential vorticity anomaly with a permanent potential vorticity anomaly. Our results suggest that small, strong vortices become trapped and circulate around the ''permanent vortex'' (or topographic feature). Although the trapped, circulating mode does not depend on $v_{\max}$, the vortex has to be strong for the nonlinear effects to maintain the vortex against dispersion. This maintenance of a small, strong vortex embedded and circulating within a larger vortex may be of importance on quite different spatial scales in problems such as the eyewall mesovortices embedded in the cyclonic circulation of tropical cyclones (Stewart and Lyons 1996; Stewart et al. 1997; Lander et al. 1999). In such a problem, trapping and weak dispersion requires a large ''vortex β Rossby number'' with the radial vorticity gradient of the circular basic state vortex replacing β, the eddy velocity replacing $v_{\max}$, and the eddy length scale replacing $r_{\max}$ (Enagonio and Montgomery 2001). The mechanism may also be relevant to mesoscale systems influenced by topography. The results have oceanographic applications as well. Oceanographers have studied similar dynamics for the effects of underwater meridional ridges on vortices (e.g., Kamenkovich et al. 1996). Vortices must be strong enough to maintain themselves against dispersion and also be in a region with weak currents. The coherency of the vortices in the ocean allows thermal and salinity anomalies to be carried far downstream.

Acknowledgments. This research was supported by grant NSC88-2111-M002-017 AP1 and NSC88-2625-Z002-029 from National Research Council of Taiwan, NSF grant ATM-9525755, and P.E. 060435N from the Office of Naval Research through the Naval Research Laboratory. We would also like to thank Drs. M. T. Montgomery and G. Carnevale and an anonymous reviewer for useful comments in the paper.

REFERENCES

Adem, J., 1956: A series solution for the barotropic vorticity equation and its application in the study of atmospheric vortices. *Tellus,* **8,** 364–372.

Bender, M. A., R. E. Tuleya, and Y. Kurihara, 1987: A numerical study of the effect of island terrain on tropical cyclones. *Mon. Wea. Rev.,* **115,** 130–155.

——, I. Ginis, and Y. Kurihara, 1993: Numerical simulations of the tropical cyclone–ocean interaction with a high-resolution coupled model. *J. Geophys. Res.,* **98,** 23 245–23 263.

Brand, S., and J. Blelloch, 1974: Changes in the characteristics of typhoons crossing the island of Taiwan. *Mon. Wea. Rev.,* **102,** 130–155.

Carnevale, G. F., G. K. Vallis, R. Purini, and M. Briscolini, 1988: Propagation of barotropic modons over topography. *Geophys. Astrophys. Fluid Dyn.,* **41,** 45–101.

——, R. C. Kloosterziel, and G. J. F. van Heijst, 1991: Propagation of barotropic vortices over topography in a rotating tank. *J. Fluid Mech.,* **233,** 119–139.

Carr, L. E., and R. T. Williams, 1989: Barotropic vortex stability to perturbations from axisymmetry. *J. Atmos. Sci.,* **46,** 3177–3191.

Chan, C. L., and R. T. Williams, 1987: Analytical and numerical studies of the beta-effect in tropical cyclone motion. Part I: Zero mean flow. *J. Atmos. Sci.,* **44,** 1257–1265.

Chang, C.-P., T.-C. Yeh, and J. M. Chen, 1993: Effects of terrain on the surface structure of typhoons over Taiwan. *Mon. Wea. Rev.,* **121,** 734–752.

Chang, S. W., 1982: The orographic effects induced by an island mountain range on propagating tropical cyclones. *Mon. Wea. Rev.,* **110,** 1255–1270.

Chu, C.-C., C.-P. Liao, and L.-H. Wang, 1998: Experimental study of a monopolar vortex moving against obstacles on a beta-plane. *Proc. Eight Int. Symp. on Flow Visualization,* Sorrento, Italy, University of Naples, 73–81.

DeMaria, M., 1996: The effect of vertical shear on tropical cyclone intensity change. *J. Atmos. Sci.,* **53,** 2076–2087.

——, and C. L. Chan, 1984: Comments on ''A numerical study of the interactions between two tropical cyclones.'' *Mon. Wea. Rev.,* **112,** 1643–1645.

Dritschel, D. G., 1998: On the persistence of non-axisymmetric vortices in inviscid two-dimensional flow. *J. Fluid Mech.,* **371,** 141–155.

Enagonio, J., and M. T. Montgomery, 2001: Tropical cyclogenesis via convectively forced vortex Rossby waves in a shallow water primitive equation model. *J. Atmos. Sci.,* **58,** 685–705.

Fiorino, M., and R. L. Elsberry, 1989: Some aspects of vortex structure related to tropical cyclone motion. *J. Atmos. Sci.,* **46,** 975–990.

Flatau, M., W. H. Schubert, and D. E. Stevens, 1994: The role of baroclinic processes in tropical cyclone motion. *J. Atmos. Sci.,* **51,** 2589–2601.

Gall, R., J. Tuttle, and P. Hildebrand, 1998: Small-scale spiral bands observed in Hurricanes Andrew, Hugo, and Erin. *Mon. Wea. Rev.,* **126,** 1749–1766.

Gill, A. E., 1977: Coastally-trapped waves in the atmosphere. *Quart. J. Roy. Meteor. Soc.,* **103,** 431–440.

Hack, J. J., and W. H. Schubert, 1986: Nonlinear response of atmospheric vortices to heating by organized cumulus convection. *J. Atmos. Sci.,* **43,** 1559–1573.

Hsu, H. H., 1987: Propagation of low-level circulation features in the vicinity of mountain ranges. *Mon. Wea. Rev.,* **115,** 1864–1892.

Ishijima, S., and M. Estoque, 1987: An observational study of orographic effects on westbound typhoon crossing Taiwan. *J. Meteor. Soc. Japan,* **65,** 4455–4467.

Kamenkovich, V. M., Y. P. Leonov, D. A. Nechaev, D. A. Byrne, and A. L. Gordon, 1996: On the influence of bottom topography on the Agulhas eddy. *J. Phys. Oceanogr.,* **26,** 892–912.

Kuo, H. C., R. T. Williams, and J. H. Chen, 1999: A possible mechanism for the eye rotation of Typhoon Herb. *J. Atmos. Sci.,* **56,** 1659–1673.

Lander, M. A., E. J. Trehubenko, and C. P. Guard, 1999: Eastern Hemisphere tropical cyclones of 1996. *Mon. Wea. Rev.,* **127,** 1274–1300.

Lin, Y. L., D. W. Hamilton, and C.-Y. Huang, 1999: Orographic influence on propagating tropical cyclones. *J. Atmos. Sci.,* **56,** 534–562.

McWilliams, J. C., and G. R. Flierl, 1979: On the evolution of isolated, nonlinear vortices. *J. Phys. Oceanogr.,* **9,** 1183–1206.

Molinari, J., S. Skubis, D. Vollaro, and F. Alsheimer, 1998: Potential vorticity analysis of tropical cyclone intensification. *J. Atmos. Sci.,* **55,** 2632–2644.

Montgomery, M. T., and R. J. Kallenbach, 1997: A theory for vortex Rossby waves and its application to spiral bands and intensity changes in hurricanes. *Quart. J. Roy. Meteor. Soc.,* **123,** 435–465.

Shapiro, L. J., 1992: Hurricane vortex motion and evolution in a three-layer model. *J. Atmos. Sci.,* **49,** 140–153.

Shieh, S. L., S. T. Wang, M. D. Cheng, and T. C. Yeh, 1998: Tropical cyclone tracks over Taiwan and its vicinity for the one hundred years 1897 to 1996 (in Chinese). Research Rep. CWB86-1M-01, Central Weather Bureau, Taipei, Taiwan, 497 pp.

Smith, G. B., and M. T. Montgomery, 1995: Vortex axisymmetrization: Dependence on azimuthal wavenumber or asymmetric radial structure changes. *Quart. J. Roy. Meteor. Soc.,* **121,** 1615–1650.

Smith, R. B., 1993: A hurricane beta-drift law. *J. Atmos. Sci.,* **50,** 3213–3215.

——, and D. F. Smith, 1995: Pseudoinviscid wake formation by mountains in shallow-water flow with a drifting vortex. *J. Atmos. Sci.,* **52,** 436–454.

——, X. Li, and B. Wang, 1997: Scaling laws for barotropic vortex beta-drift. *Tellus,* **49A,** 474–485.

Stewart, S. R., and S. W. Lyons, 1996: A WSR-88D radar view of Tropical Cyclone Ed. *Wea. Forecasting,* **11,** 115–135.

——, J. Simpson, and D. Wolff, 1997: Convectively-induced mesocyclonic vortices in the eyewall of tropical cyclones as seen by WSR-88D doppler radars. Preprints, *22d Conf. on Hurricanes and Tropical Meteorology,* Fort Collins, CO, Amer. Meteor. Soc., 106–108.

Sutyrin, G. G., and G. R. Flierl, 1994: Intense vortex motion on the beta plane: Development of the beta gyres. *J. Atmos. Sci.,* **51,** 773–790.

Wang, S. T., 1980: Prediction of the behavior and intensity of typhoons in Taiwan and its vicinity (in Chinese). Research Rep. 108, Chinese National Science Council, Taipei, Taiwan, 100 pp.

Wurman, J., and J. Winslow, 1998: Intense sub-kilometer-scale boundary layer rolls observed in Hurricane Fran. *Science,* **280,** 555–557.

Yeh, T. C., and R. L. Elsberry, 1993a: Interaction of typhoons with the Taiwan orography. Part I: Upstream track deflections. *Mon. Wea. Rev.,* **121,** 3193–3212.

——, and ——, 1993b: Interaction of typhoons with the Taiwan orography. Part II: Continuous and discontinuous tracks across the island. *Mon. Wea. Rev.,* **121,** 3213–3233.

Zehnder, J. A., 1993: The influence of large-scale topography on barotropic vortex motion. *J. Atmos. Sci.,* **50,** 2519–2532.